Solar Energy 173 (2018) 993–1001

Contents lists available at ScienceDirect

Solar Energy

journal homepage: www.elsevier.com/locate/solener

Inertial impaction and surface diffusion-assisted rapid dye molecule adsorption on TiO_2 thin films for highly efficient dye-sensitized solar cells

Yaojia Zhang[a], Ji Hoon Kim[a,b], Xiuting Luo[a], Soo Hyung Kim[a,b,c,*]

[a] Department of Nanofusion Technology, Pusan National University, 2, Busandaehak-ro 63beon-gil, Geumjeong-gu, Busan 46241, Republic of Korea
[b] Research Center for Energy Convergence Technology, Pusan National University, 2, Busandaehak-ro 63beon-gil, Geumjeong-gu, Busan 46241, Republic of Korea
[c] Department of Nano Energy Engineering, Pusan National University, 2, Busandaehak-ro 63beon-gil, Geumjeong-gu, Busan 46241, Republic of Korea

ARTICLE INFO

Keywords:
Aerosol impactor
Surface diffusion
Dye adsorption
Dye-sensitized solar cells

ABSTRACT

An effective and versatile single-stage aerosol impactor was specially designed to rapidly coat the surface of TiO_2 thin films with a controlled amount of dye molecules via inertial impaction and surface diffusion to speed-up the manufacturing process and enhance the photovoltaic performance of dye-sensitized solar cells (DSSCs). By theoretically determining the specific dimensions of the aerosol accelerating nozzle and experimentally controlling the mixing ratio between the sheath gas and dye aerosol flow rates in the single-stage aerosol impactor, the speed and quality of dye adsorption on the TiO_2 thin films of the photoelectrodes could be systematically assessed in terms of the photovoltaic performance of the DSSCs, including open-circuit voltage, short-circuit current, fill factor, and power conversion efficiency (PCE). It was found that the aerosol impactor-assisted dye coating method developed in this study significantly reduced the duration of dye adsorption (aerosol coating duration = 20–60 min) and increased the PCE of the DSSCs to 7.28%. Using this methodology, dye-coating was ~20 times faster and the fabricated device has 23% higher PCE compared to the DSSC fabricated by the conventional dip coating method (dip-coating duration = 1200 min, PCE = 5.92%). These results proved that the single-stage aerosol impactor designed in this study is a very effective and versatile device for rapidly coating the surface of TiO_2 thin films with dye molecules using sufficient inertial impaction, which enables the introduced dye molecules to infiltrate and quickly adsorb on the surface of TiO_2 nanoparticles accumulated in the DSSC photoelectrodes.

1. Introduction

The photovoltaic performance of dye-sensitized solar cells (DSSCs) composed of dye-adsorbed TiO_2 nanoparticle (NP)-accumulated photoelectrodes formed on a fluorine-doped tin oxide (FTO) conducting substrate (O'Regan and Gratzel, 1991; Ahn et al., 2013, 2014; Luo et al., 2016, 2017; Latini et al., 2013; Green et al., 2009; Liu et al., 2006; Moon et al., 2013; Lee et al., 2010; Krkrek et al., 2006), Pt-coated FTO conducting substrate as a counter electrode (Li et al., 2008; Ahn et al., 2014; Wang and Hu, 2012), and redox electrolyte filled between the two electrodes (Wu et al., 2008; Ahn et al., 2012) have been greatly improved in the years following the first report by Gräzel et al. (O'Regan and Gratzel, 1991). DSSCs have the advantages of relatively low manufacturing cost, simple manufacturing process, and relatively high power conversion efficiency (PCE). Therefore, DSSCs are considered as promising candidates for next-generation solar cells that can enable green energy production on a large scale. The general working principle of DSSCs is that the solar energy is converted into electric energy with the assistance of dye sensitizer. In the photoelectrode, electrons are generated by dye molecules attached on the surface of TiO_2 semiconductors, which absorb the incident photons. This form of photoexcitation indicates that the electrons are excited from the highest occupied molecular orbital (HOMO) to the lowest unoccupied molecular orbital (LUMO). Since the LUMO energy level of dye molecules is greater than that of conduction band of TiO_2, the photogenerated electrons are rapidly injected into TiO_2 layer, where the dye molecules are oxidized. The photogenerated electrons diffuse through the external circuits, and they reach to the counter electrode. Finally they transfer to the liquid electrolyte, where the oxidized dye molecules participate in a redox reaction and are restored back to their ground state. Meanwhile I^- ions are oxidized to I_3^- ions, and the I_3^- ions diffuse toward the counter electrode and accept the photogenerated electrons so that they

* Corresponding author at: Department of Nano Energy Engineering, Pusan National University, 2, Busandaehak-ro 63beon-gil, Geumjeong-gu, Busan 46241, Republic of Korea.
E-mail address: sookim@pusan.ac.kr (S.H. Kim).

https://doi.org/10.1016/j.solener.2018.08.052
Received 29 May 2018; Received in revised form 17 August 2018; Accepted 20 August 2018

are reduced back to I^- ions.

Several research groups have performed in-depth studies on the various components of DSSCs to improve their photovoltaic performances. Toward this end, a major strategy is to increase the specific surface area of the TiO_2 NP-accumulated photoelectrode so that it may adsorb more dyes that generate electrons under sunlight irradiation (Yan et al., 2011; Mohamed et al., 2016; Yu et al., 2009; Kim et al., 2013). The other strategy is to tune the nanostructures of the TiO_2 NP-accumulated photoelectrode and improve the efficiency of electron transfer so that the recombination rate of the photogenerated electrons with liquid electrolyte is reduced (Hossain et al., 2015; Wu et al., 2014, 2012; Liao et al., 2011; Su et al., 2017; Lee et al., 2015).

Among the various components of DSSCs, the fabrication of photoelectrodes takes a relatively long time because of the tedious dye adsorption process. One of the most important attributes of the DSSC photoelectrodes is their ability to adsorb a sufficient amount of dye molecules on the surface of TiO_2 NPs. In general, photoelectrodes in DSSCs are made up of TiO_2 NP-accumulated thin films that are formed on an FTO glass using a screen-printing process, and then immersed into a dye solution for > 10–36 h to ensure adequate dye adsorption (Jasim, 2011; Tesfamichael et al., 2003). This traditional dye adsorption made possible by the dip coating process results in the slow fabrication of DSSCs and the consumption of an unpredictable amount of the dye molecules. Consequently, it is hard to sustain a stable photovoltaic performance of the resulting DSSCs that are fabricated by the dip coating process. In order to achieve a rapid dye-adsorption process during DSSC fabrication, several research groups have tried to increase the dye-adsorption rate by increasing the dye diffusion flux considerably by using highly concentrated dye solutions at relatively high temperature conditions (Noda et al., 2009; Hinsch et al., 2011). However, all of these approaches have limitations in realizing controlled dye adsorption. We also employed an electrospray process so that a rapid dye adsorption in the aerosol phase was successfully realized (Luo et al., 2016), but it has several disadvantages of requiring complex and expensive high electric power circuit system and difficulties in scale-up process.

In this study, we specially designed and manufactured a single-stage dye aerosol impactor to rapidly deposit dye molecules on the surface of TiO_2 NP-accumulated thin films via inertial impaction under controlled fluid flow, which enabled us to eventually rapidly fabricate DSSCs that demonstrated stable and sustainable photovoltaic performance. Briefly, the dye solution was transformed into dye-containing droplets using an ultrasonic atomizer, which were then accelerated in the specially designed single-stage aerosol impactor so that they collided with the surface of the TiO_2 thin film with strong momentum. Under the optimized carrier gas flow conditions, the major dye aerosols were impacted in such a manner that they became attached and diffused throughout the TiO_2 thin film. Finally, we have demonstrated that the rapid dye adsorption process was successfully implemented on the surface of TiO_2 thin films. Additionally, the effect of rapid dye adsorption on the photovoltaic performance of DSSCs was systematically investigated.

2. Materials and methods

2.1. Design and manufacture of single-stage dye aerosol impactor

Inertial impaction is a special case in curvature motion that allows the collection and measurement of aerosol particles. Single-stage aerosol impactors have been widely used for separating aerosol particles that are larger than a certain size by inertial impaction (Marple and Klaus, 1976). Fig. 1a shows the operating principle of a single-stage impactor. Briefly, when aerosol particles are introduced into an impactor nozzle at a specific flow rate, they accelerate toward an impaction plate placed at the bottom of the impactor. The impaction plate deflects the flow to form an abrupt 90° bend in the streamline. Among the introduced particles, those that have inertia exceeding a certain value, are unable to follow the streamlines and collide on the surface of the impaction plate. However, when the introduced particles are smaller, they cannot reach the impaction plate because of lower momentum. These particles avoid hitting the impaction plate and can be finally exhausted by following the streamlines of the carrier gas flow or collected for recycling in a trap installed in the exhausting streamlines. A single-stage aerosol impactor for depositing dyes was specially designed in the present study and is shown in Fig. 1b and c. It consisted of a cover plate with an aerosol inlet, accelerating nozzle, and impaction plate with two aerosol outlets. The aerosol inlet was located at the center of the cover plate. The accelerating nozzle was 1 cm in width and 5 cm in length. The rubber O-rings were inserted at the connecting part between the nozzle and the cover and the base of the impactor to prevent gas leakage. In addition, bolts installed at the base plate were used to support individual parts and simultaneously increased the air tightness. The gas outlets were finally connected to an external vacuum pump to eliminate the undeposited dye aerosols and carrier gas in the exhaust.

Fig. 2 shows the schematics of the entire experimental system. The first step in this process was the preparation of dye aerosols Fig. 2a), which were generated from the dye solution using an ultrasonic atomizer operated at a power of 40 W and frequency of 20 Hz. Here, the concentration of the dye solution, i.e., Ru-dye $(Bu_4N)_2[Ru(Hdcbpy)_2(NCS)_2]$ (N719, Solaronix, SA, Switzerland), was ~0.3 mM. In the second step, the dye aerosol was deposited on the substrate Fig. 2b). The TiO_2 thin film-coated FTO glass was placed on the impaction plate. The center of the TiO_2 thin film was geometrically aligned with that of the aerosol accelerating nozzle. The dye aerosols introduced through the nozzle with high momentum collided with the surface of the film and then rapidly diffused into the TiO_2 thin film. The smaller dye aerosols with relatively low momentum were unable to collide with the surface of the TiO_2 thin film and were exhausted along with the carrier gas through the aerosol outlets. Fig. 2c shows the schematics of the entire dye aerosol coating system employed in this study. It was mainly composed of a gas filter and a silica-gel dryer, mass flow controllers, an ultrasonic atomizer, a single-stage aerosol impactor, and a vacuum pump. Filtered and dried air was provided for aerosol and sheath flows. The aerosol and sheath flow rates were precisely controlled using mass flow controllers (Model No. MPR2000, MKP). The dye aerosol concentration was controlled by varying the mixing ratio of aerosol and sheath flows, and the generated dye aerosols were finally introduced into the single-stage impactor for coating TiO_2 thin film-based photoelectrodes of DSSCs.

To design and manufacture the single-stage aerosol impactor, various parameters such as Stokes number (*Stk*), Reynolds number (*Re*), *S/W*, and *T/W* (where, *S* is the distance between the accelerating nozzle and the impaction plate, *W* is the nozzle width, and *T* is the throat length of nozzle), were taken into account. *Stk* is a dimensionless number defined by the ratio of the stop distance of the aerosol particle to the radius of the nozzle neck as given in Eq. (1), indicating whether an aerosol particle would be collected by colliding with the surface of the impaction plate (Marple and Klaus, 1976; Mehdizadeh et al., 2013; Fuchs, 1989).

$$Stk = \frac{\rho_p V_o C D_p^2 / 18\mu}{W/2} \quad (1)$$

where ρ_p refers to the particle density, V_o is the average velocity of fluid flow in the nozzle, C stands for the Cunningham slip correction factor, D_p corresponds to the average particle diameter, and μ is the viscosity of the fluid.

Re is a dimensionless number defined by the ratio of fluid inertia and viscous force, as given in Eq. (2).

$$Re = \frac{\rho V_0 W}{\mu} \quad (2)$$

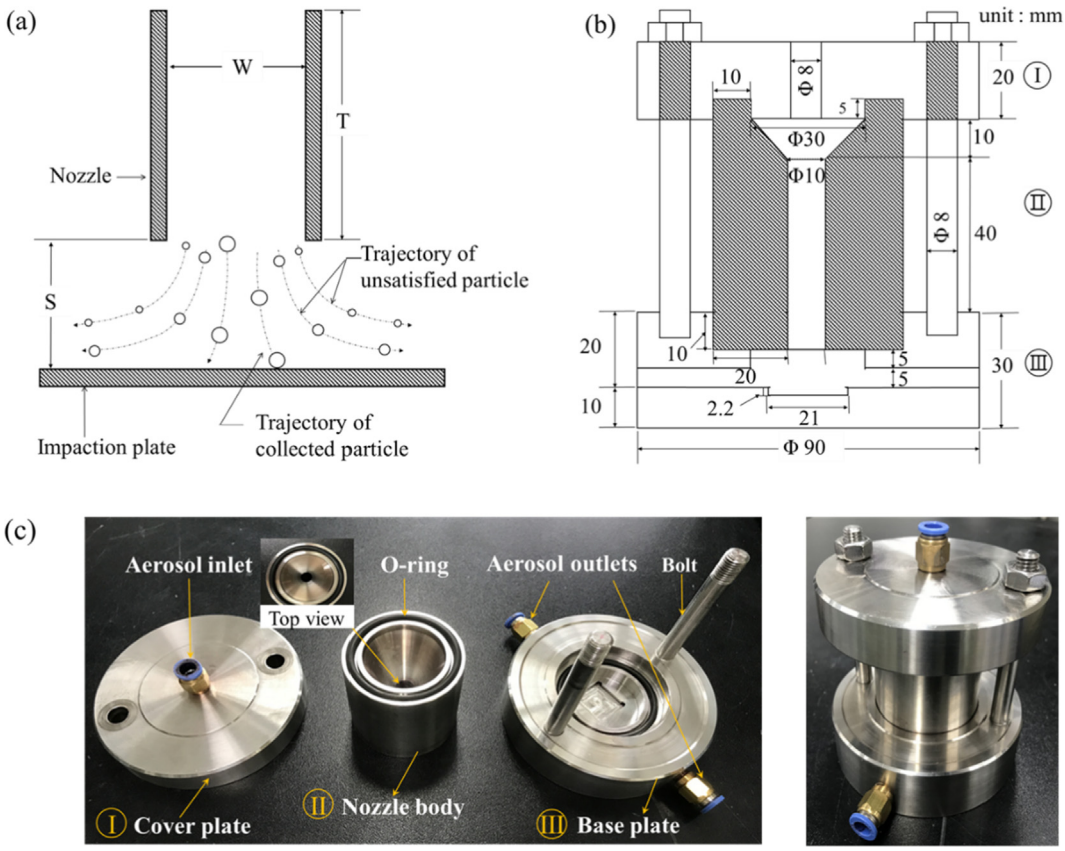

Fig. 1. Schematics of the (a) operating principle and (b) specific design and dimensions of a single-stage dye aerosol impactor. (c) Photographs of individual parts (left) and the completely assembled single-stage dye aerosol impactor (right).

where ρ denotes the density of the fluid.

Here, V_o can be simply expressed by the volumetric flow rate divided by the nozzle area (i.e., $V_o = 4Q/\pi W^2$, Q is the volumetric flow rate). Thus, *Stk* and *Re* can be rewritten as follows:

$$Stk_{50} = \frac{4\rho_p Q C D_{50}^2}{9\pi\mu W^3} \tag{3}$$

where D_{50} indicates when a sample of the cumulative size distribution percentage reaches 50% of the corresponding particle size, and is commonly used as the average particle size.

$$Re = \frac{4\rho Q}{\pi\mu} \tag{4}$$

From Eqs. (3) and (4), the nozzle width is obtained as a function of *Re* and *Stk* as given in Eq. (5).

$$W = \sqrt{\frac{\rho_p Re}{9\rho Stk_{50}}}\sqrt{C}D_{50} \tag{5}$$

Here, Stk_{50} refers to the Stokes number at 50% collection efficiency and indicates the location of the ideal cutoff curve that best fits the actual cutoff curve. Ideal cutoff curve implies that all particles larger than a certain size are collected on the impaction plate and all particles smaller than that size pass through. For a circular nozzle impactor, Stk_{50} is known to be ~0.24, which is independent of the nozzle diameter and flow velocity (i.e., $(Stk_{50})^{1/2} = 0.49$) (Marple and Klaus, 1976; Rader and Marple, 1985; Hinds, 1999).

The value of *Re* was fixed as ~3000 throughout this study for the aerosol particles to have sufficient inertial impaction without turbulence ($Re \gg 3000$) or relatively low inertial impaction ($Re \ll 3000$) (Slezakova and Morais, 2012). On the basis of these specific parameters, including $\rho = 1.205 \times 10^{-3}\,g\,cm^{-3}$ (air density), $\rho_p = 0.789\,g\,cm^{-3}$ (ethanol density), $\sqrt{C}\,D_{50} = \sim 10\,\mu m$, and $Re = 3000$, the resulting width of the round nozzle in the single-stage aerosol impactor was calculated to be ~1 cm. In addition, the values of $S/W = 1$ and $T/W = 5$ were chosen in this study because they were previously found by other research groups to maintain sharp cutoff characteristics and stable cutoff size of the aerosol particles (Marple and Klaus, 1976; Rader and Marple, 1985). Therefore, the specific dimensions of the impactor designed in the present study were finally determined to be $W = \sim 1$ cm, $S = \sim 1$ cm, and $T = \sim 5$ cm for $Q = \sim 25\,L\,min^{-1}$ and $D_p = \sim 10\,\mu m$, whereby the dye aerosols could be collected on the TiO_2 thin films of the photoelectrodes used in DSSCs.

2.2. Fabrication of the photoelectrode and counter electrode of DSSCs

The photoelectrode of DSSCs was composed of the TiO_2 thin film and FTO glass (SnO_2:F, 7 Ω/sq, Pilkington, Boston, USA). The TiO_2 thin film was prepared by a screen-printing process using TiO_2 paste. For preparing the TiO_2 paste, 0.3 g of commercial TiO_2 NPs (P25, Degussa, Germany), 1 g of terpineol, and 0.05 mL of acetic acid (CH_3COOH) were mixed in 3 mL of ethanol in a vial. In another vial, 0.15 g of ethyl cellulose was dispersed in 5 mL of ethanol and sonicated for 1 h. Both of these solutions were then mixed using a planar mixing machine (Awatori Rentaro ARE-310, Thinky Corporation, Japan) for 3 min at 2000 rpm. The mixed solution was heated to remove the ethanol and a viscous TiO_2 paste was obtained. Before performing the screen-printing process, FTO glasses were cleaned with acetone, ethanol, and deionized water in an ultrasonic bath for 20 min to remove impurities. The cleaned FTO glasses were then pretreated with $TiOCl_2$ solution, which consisted of 0.247 mL of $TiOCl_2$ and 20 mL of deionized water, to enable strong adhesion of the TiO_2 thin films onto the surface of the FTO glass. This pretreatment process lasted for 30 min at 70 °C and subsequently, the $TiOCl_2$-treated FTO glasses were heated at 500 °C for

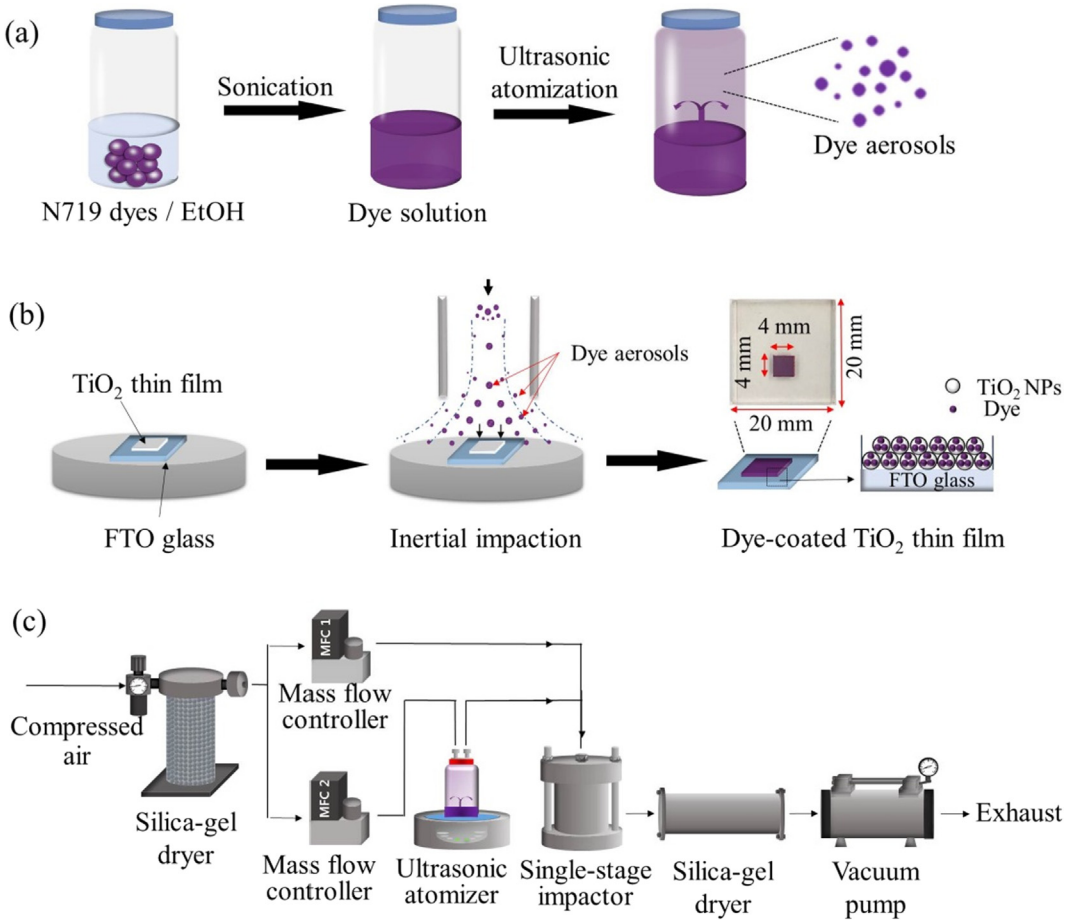

Fig. 2. Schematics of (a) generation of the dye aerosols, (b) coating process of the dye aerosols on the surface of the TiO_2 thin film by inertial impaction, and (c) the complete experimental set-up of a single-stage dye aerosol impactor system.

30 min in an electric furnace. After the above mentioned preparation steps were implemented, TiO_2 thin films were deposited on the $TiOCl_2$-treated FTO glasses as an electron transfer layer using the screen-printing process with an approximately 20 μm thick and 0.4 cm × 0.4 cm photoactive area. Subsequently, the screen-printed substrate was heated at 500 °C for 30 min for sintering the TiO_2 primary particles in the thin films.

For the dye adsorption process, we first employed a standard atomizer (Model No. LH-7321FN, Cuckoo, Korea) to generate dye aerosol droplets as shown in Fig. 2. The dye aerosol was then carried into the accelerating nozzle of a single-stage aerosol impactor by carrier air flow. The gas flow rate was controlled using mass flow controllers (MFC) (Mkp, Model No. MPR2000, Korea). When the dye aerosol-laden air flow encountered the impaction plate, its direction was abruptly changed. Simultaneously, this resulted in a significant change in the trajectories of the dye aerosol droplets. The aerosol droplets that were larger than the critical cutoff size were deviated from the carrier gas flow and finally collided with the TiO_2 thin films installed on the impaction plate. The dye aerosols directly hit the surface of the TiO_2 thin film and then rapidly penetrated through the interstitial spaces among the TiO_2 NPs. The dye molecules were then combined with the TiO_2 thin films via chemical interactions between the hydroxyl (−OH) groups of TiO_2 and the carboxylate (−COOH) groups of the dye molecules, resulting in ester linkages (−COOR) (Luo et al., 2016; Newton et al., 1997; Kuo and Wu, 2014). The dye aerosol droplets that were smaller than the critical size were laden by the carrier gas and collected by a filter operated by vacuum pump.

For preparing the counter electrodes of DSSCs, FTO glasses were drilled with two holes for subsequent injection of the liquid electrolyte (AN-50, Solaronix, SA, Switzerland). The glasses were cleaned according to the above sonication cleaning steps and then coated with Pt by ion sputtering (Model No. E1010, Hitachi, Chiyoda-ku, Japan) for improving the electrical conductivity.

2.3. Assembly and photovoltaic performance measurement of DSSCs

The assembly of the both the photoelectrode and the counter electrode of DSSCs requires a hot-melt polymer film (60 μm thickness, Surlyn, DuPont, USA). The hot-melt polymer was cut into a hollow rectangle of a suitable size. It was then put on the photoelectrode to ensure that the dye-coated TiO_2 thin film fitted inside the hollow square. The counter electrode was then placed on the hot-melt polymer. Finally, a sandwich structure of the photoanode/polymer film/counter electrode was formed and heated at 120 °C for 4 min under a pressurized force for tight sealing. Subsequently, the liquid electrolyte was injected through the drilled holes of the counter electrode and the holes were finally sealed using a hot-melt polymer and cover glass.

The photovoltaic performances of the DSSCs were recorded using a solar simulator (PEC-L11, Peccell Technologies, Inc., Kanagawa, Japan) at the condition of 1.5 air mass and 1 sun (=100 mW cm^{-2}) illumination. The current density-voltage (*J-V*) curves and electrochemical impedance spectra (EIS) were automatically measured by the Keithley SMU 2400 source meter (Cleveland, OH, USA). To measure the amount of dye, TiO_2 thin film-coated FTO glass was immersed in 0.1 mol L^{-1} NaOH solution (deionized water:ethanol = 1:1) to dissolve the dye molecules adsorbed by the TiO_2 thin films. Next, the dye-containing solution was examined using an ultraviolet–visible (UV–Vis) spectrometer (Cary 5000, Agilent, Englewood, CA, USA) to analyze the

Table 1
Summary of the photovoltaic performances of the DSSCs fabricated using a dye aerosol coating method under different mixing ratios of sheath and dye aerosol flow rates.

Ratio of flow rate (Sheath:Aerosol)	J_{sc}* (mA cm^{-2})	V_{oc}* (V)	FF*	PCE* (%)
5:20	11.96 ± 0.33	0.71 ± 0.01	0.72 ± 0.04	6.12 ± 0.27
10:15	12.75 ± 0.70	0.69 ± 0.02	0.72 ± 0.02	6.31 ± 0.30
15:10	13.28 ± 0.57	0.71 ± 0.01	0.71 ± 0.03	6.69 ± 0.21
20:5	13.79 ± 0.62	0.74 ± 0.01	0.71 ± 0.02	7.18 ± 0.12
22:3	11.14 ± 0.51	0.66 ± 0.02	0.71 ± 0.02	5.22 ± 0.18
24:1	4.02 ± 0.45	0.62 ± 0.03	0.72 ± 0.05	1.80 ± 0.21

* Note: Unit of flow rate: L min^{-1}, J_{sc}: short circuit current density, V_{oc}: open circuit voltage, FF: fill factor, PCE: power conversion efficiency.

absorbance of dye N719 (Angelis et al., 2010). The incident photon-to-electron conversion efficiency (IPCE) was measured with the solar simulator (Abet Technologies Inc., Sun 20009), which used an arc lamp light source (Abet Technologies Inc., LS-150-Xe).

3. Results and discussion

The effect of the mixing ratio of sheath air and dye aerosol flow rates (or dye aerosol concentration) on the photovoltaic performance of the DSSCs was investigated to determine the optimized operating conditions of the dye aerosol impactor. The inertial impaction of dye aerosol droplets on the surface of TiO_2 thin film was fixed for ~30 min. Consequently, the short circuit current density (J_{sc}) and power conversion efficiency (PCE) values of the DSSCs increased with the increasing sheath air flow rate up to 20 L min^{-1} and simultaneously decreased the dye aerosol flow rate down to 5 L min^{-1} Table 1). However, there were no appreciable changes in the open circuit voltage (V_{oc}) and fill factor (FF) for the cases of aerosol flow rates of 5–20 L min^{-1}. For the highest aerosol concentrations (sheath:aerosol = 5:20), the dye aerosol droplets were continuously accumulated on the surface of the TiO_2 thin film, which turned into an entirely wet surface covered with the dye solution. This resulted in shielding the direct impaction of the continuously introduced dye aerosol droplets on the surface of the TiO_2 thin film. When the dye aerosol flow rate reached ~15 L min^{-1} (sheath:aerosol = 10:15) with lesser aerosol concentration, the degree of wetness of the TiO_2 thin film decreased qualitatively to some extent. As the dye aerosol flow rate was reduced further to ~10 L min^{-1} (sheath:aerosol = 15:10), the surface of the TiO_2 thin film was not wet because of the rapid evaporation of the aerosol solvent, implying that the dye molecules were effectively adsorbed by aerosol impaction. When the dye aerosol flow rate was reduced to ~5 L min^{-1} (sheath:aerosol = 20:5), the photovoltaic performance of the resulting DSSC was found to be the best. However, when the dye aerosol flow rate was further reduced to less than ~5 L min^{-1} (sheath:aerosol = 22:3 & 24:1), the photovoltaic performance of the resulting DSSC was found to be decreased due to lack of dye molecules coated on the TiO_2 thin films. Therefore, the mixing ratio of sheath and aerosol was fixed to 20:5 as the optimized flow rate condition for maximizing the dye aerosol coating efficiency and photovoltaic performance of DSSCs.

We also investigated the effect of aerosol coating duration on the photovoltaic performances of the DSSCs at the optimized sheath and dye aerosol flow rate condition (sheath:aerosol = 20:5). For comparison, we also prepared DSSCs fabricated by the conventional dip coating method for varying time durations of the dye adsorption process Table 2). As the duration of dye adsorption was increased in both dip and aerosol coating processes, the amount of the adsorbed dye (M_{DA}), J_{sc}, and PCE were also increased. In the case of conventional dip coating duration of 1200 min, the resulting $M_{DA,}$ J_{sc}, and PCE of the fabricated DSSCs were 10.58×10^{-6} mol cm^{-2}, 11.29 mA cm^{-2}, and 5.92%, respectively. For the dip coating duration longer than longer than 1800 min, the resulting PCE was saturated at ~6.2% in the present study. However, in the case of aerosol coating performed for 60 min, the resulting M_{DA}, J_{sc}, and PCE of the DSSCs were considerably increased to 15.55×10^{-6} mol cm^{-2}, 15.54 mA cm^{-2}, and 7.28%, respectively. The resulting PCE was saturated at ~7.3% after the aerosol coating duration of ~30 min. This suggests that the dye aerosol coating method using the single-stage dye aerosol impactor employed in the present study was very effective and could significantly shorten the tedious traditional dip-coating dye adsorption process. The inertial impactor system imparted high momentum to the dye aerosol droplets, such that they then rapidly impacted the TiO_2 thin film and were quickly adsorbed because of their enhanced surface and intra-particle diffusion rates (Kuo and Wu, 2014; Yu et al., 2010). In contrast; the TiO_2 thin film was immersed in a dye solution in the conventional dip coating method, where the dye molecules diffused very slowly and were adsorbed to the surface of TiO_2 thin film as a result of a dye concentration gradient in between the dye solution and TiO_2. In both dye adsorption methods, V_{oc} increased with the increasing the dye coating duration until the dye adsorptions were saturated. A gradual increase in V_{oc} was observed for the dip coating method, while a rapid increase in V_{oc} was observed for aerosol coating method owing to the high dye adsorption rate.

Fig. 3a and b show the J-V curves of the DSSCs fabricated by 'the dip coating and aerosol coating methods for different coating durations. The maximum J_{sc} value clearly increased as the coating duration increased. This is because the amount of dye molecules adsorbed on the photoelectrode also increased and upon irradiation of the DSSCs, the dye molecules generated more photoelectrons. The Nyquist plots in Fig. 3c and d commonly show three semicircles. The first semicircle from the left represents the resistance between the Pt counter electrode and the liquid electrolyte. The second semicircle represents the recombination resistance (R_{rec}), which is the resistance at the dye/TiO_2/electrolyte interfaces. The third semicircle represents the resistance of the liquid electrolyte. The R_{rec} of the DSSCs fabricated by the aerosol coating method was observed to be smaller than that of the DSSCs fabricated by the dip coating method. It was because more dye molecules were effectively adsorbed by the latter method on the TiO_2 thin film of the DSSCs in such a short time, which resulted in the injection of more electrons through the TiO_2 film so that higher J_{sc} and lower R_{rec} were obtained. The electron transport resistance (R_t) includes two components (Bisquert and Santiago, 2009; Ha et al., 2016), namely, among TiO_2 NPs and between TiO_2 thin film and the FTO glass. It can be calculated from the relation given in Eq. (6),

$$\frac{R_t}{3} + R_{rec} = R_{total} \tag{6}$$

where R_{total} is the total resistance of DSSC. The magnitudes of R_t of the DSSCs fabricated by the aerosol coating method was higher than that of DSSCs fabricated by the dip coating method. This was presumably because the photogenerated electrons met with more resistance as a result of highly aggregated dye molecules on the surface of the TiO_2 thin film, which will be discussed later in detail (see Fig. 4). Fig. 3e and f show the Bode plots for the assembled DSSCs. The characteristic frequency peaks in the Bode phase angle represent the delayed phase in terms of capacitance and the lifetime of electrons (τ_e), which can be calculated from Eq. (7).

$$\tau_e = \frac{1}{2\pi f_{max}} \tag{7}$$

Here, $f_{\max}$ is the maximum peak frequency. The value of τ_e was found to increase with the increasing coating duration for both dip and aerosol coating processes. The increase in τ_e suggested that a smaller effective recombination rate constant for the electrons and the liquid electrolyte implied a greater probability of the electrons passing through the TiO_2 semiconductor to the Pt counter electrode and consequently higher values of J_{sc} and PCE of the fabricated DSSCs.

Table 2
Summary of photovoltaic performances of the DSSCs fabricated using both dip coating and aerosol coating methods for different dye deposition durations.

Dye-adsorption method	Time (min)	M_{DA}* (10^{-6} mol cm^{-2})	J_{sc} (mA cm^{-2})	V_{oc} (V)	*FF*	*PCE* (%)	R_{rec}* (Ω)	R_t* (Ω)	τ_e* (ms)
Dip coating	60	1.56 ± 0.21	6.59 ± 0.31	0.66 ± 0.01	0.74 ± 0.01	3.19 ± 0.10	25.76	51.78	4.00
	300	5.28 ± 0.18	9.91 ± 0.58	0.68 ± 0.01	0.73 ± 0.01	4.92 ± 0.07	19.62	46.08	4.00
	600	9.60 ± 0.20	10.75 ± 0.64	0.70 ± 0.01	0.73 ± 0.02	5.56 ± 0.13	20.69	45.78	5.04
	1200	10.58 ± 0.14	11.29 ± 0.41	0.72 ± 0.01	0.72 ± 0.01	5.92 ± 0.08	18.51	54.84	6.34
	1800	10.97 ± 0.23	11.96 ± 0.29	0.72 ± 0.01	0.71 ± 0.01	6.12 ± 0 .11	18.38	47.40	6.34
Aerosol coating	5	1.12 ± 0.30	6.39 ± 0.69	0.63 ± 0.01	0.74 ± 0.02	3.00 ± 0.19	23.04	60.57	4.00
	10	5.12 ± 0.27	10.54 ± 0.73	0.68 ± 0.02	0.73 ± 0.01	5.25 ± 0.27	17.99	59.55	4.00
	20	11.96 ± 0.37	13.37 ± 0.55	0.70 ± 0.01	0.70 ± 0.01	6.53 ± 0.22	17.96	58.74	7.98
	30	14.90 ± 0.29	13.79 ± 0.62	0.74 ± 0.01	0.71 ± 0.02	7.18 ± 0.12	17.02	61.98	7.98
	40	15.51 ± 0.14	14.56 ± 0.63	0.71 ± 0.02	0.68 ± 0.02	7.05 ± 0.06	16.66	58.76	10.05
	60	15.55 ± 0.34	15.44 ± 0.57	0.69 ± 0.01	0.68 ± 0.01	7.28 ± 0.11	16.67	57.63	10.05

* Note: M_{DA}: amount of dye adsorbed, R_{rec}: recombination resistance, R_t: transport resistance, τ_e: electron life time.

Fig. 4 shows the SEM images of the photoelectrodes in cross-sectional view prepared for different dye coating durations. Fig. 4a and b show the TiO_2 NPs accumulated-thin film photoelectrode without the coating dye molecules. The TiO_2 NPs were uniformly attached to the surface of FTO glass. Fig. 4c shows the case of TiO_2 thin film fabricated by dye aerosol coating for a duration of 10 min, after which the dye molecules were unevenly covered over the TiO_2 thin film because of the relatively short aerosol coating duration. In addition, it was observed that the dye molecules could not sufficiently infiltrate the TiO_2 thin film in-depth as shown in Fig. 4d. However, upon dye aerosol coating for 30 and 60 min, as shown in Fig. 4e, f, g, and h, the dye molecules seemed to completely penetrate through the TiO_2 thin film so that the TiO_2 NPs

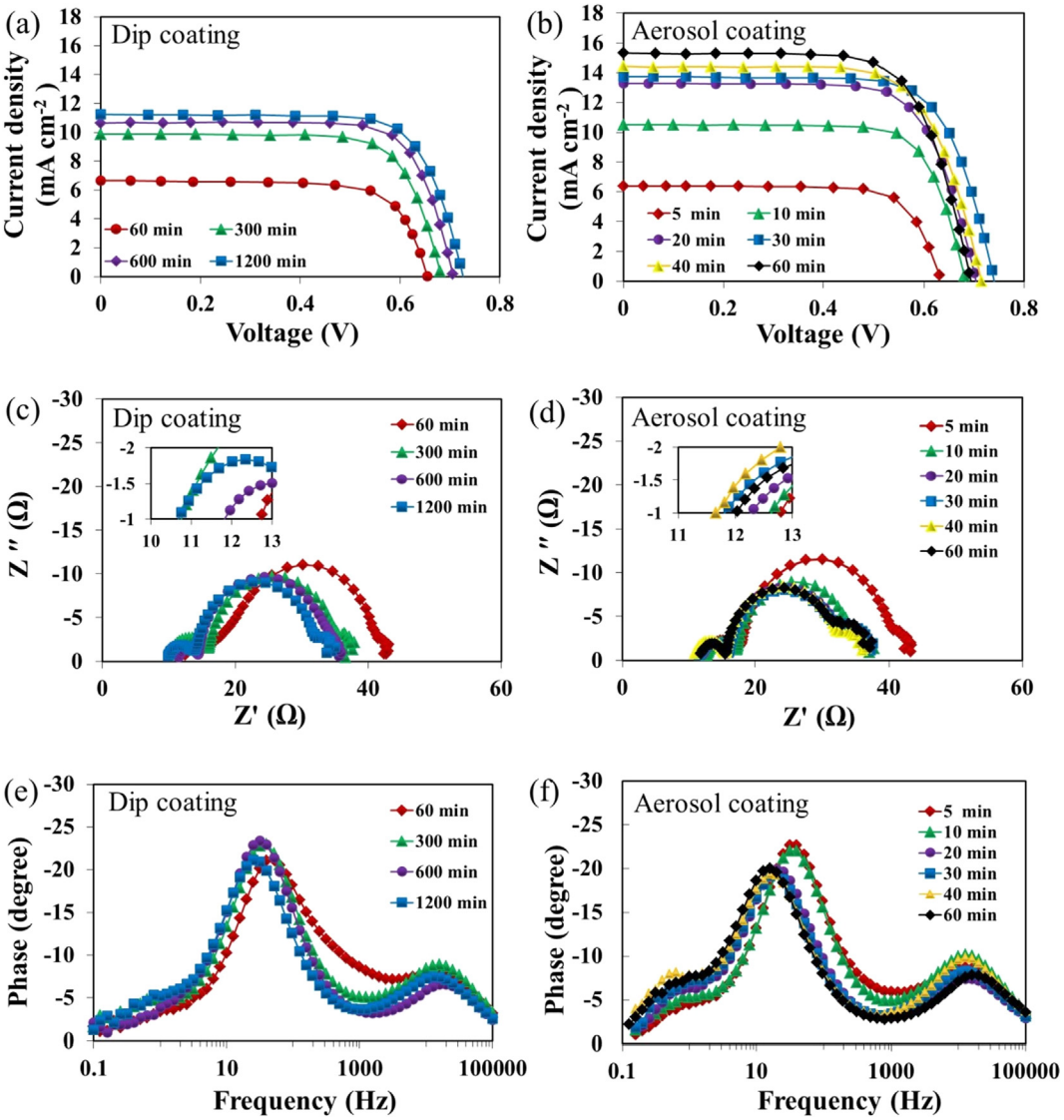

Fig. 3. (a) *J-V* curves, (c) Nyquist plots, and (e) Bode plots of the DSSCs fabricated using the dip coating method for different coating durations. (b) *J-V* curves, (d) Nyquist plots, and (f) Bode plots of the DSSCs fabricated using the aerosol coating method for different coating durations.

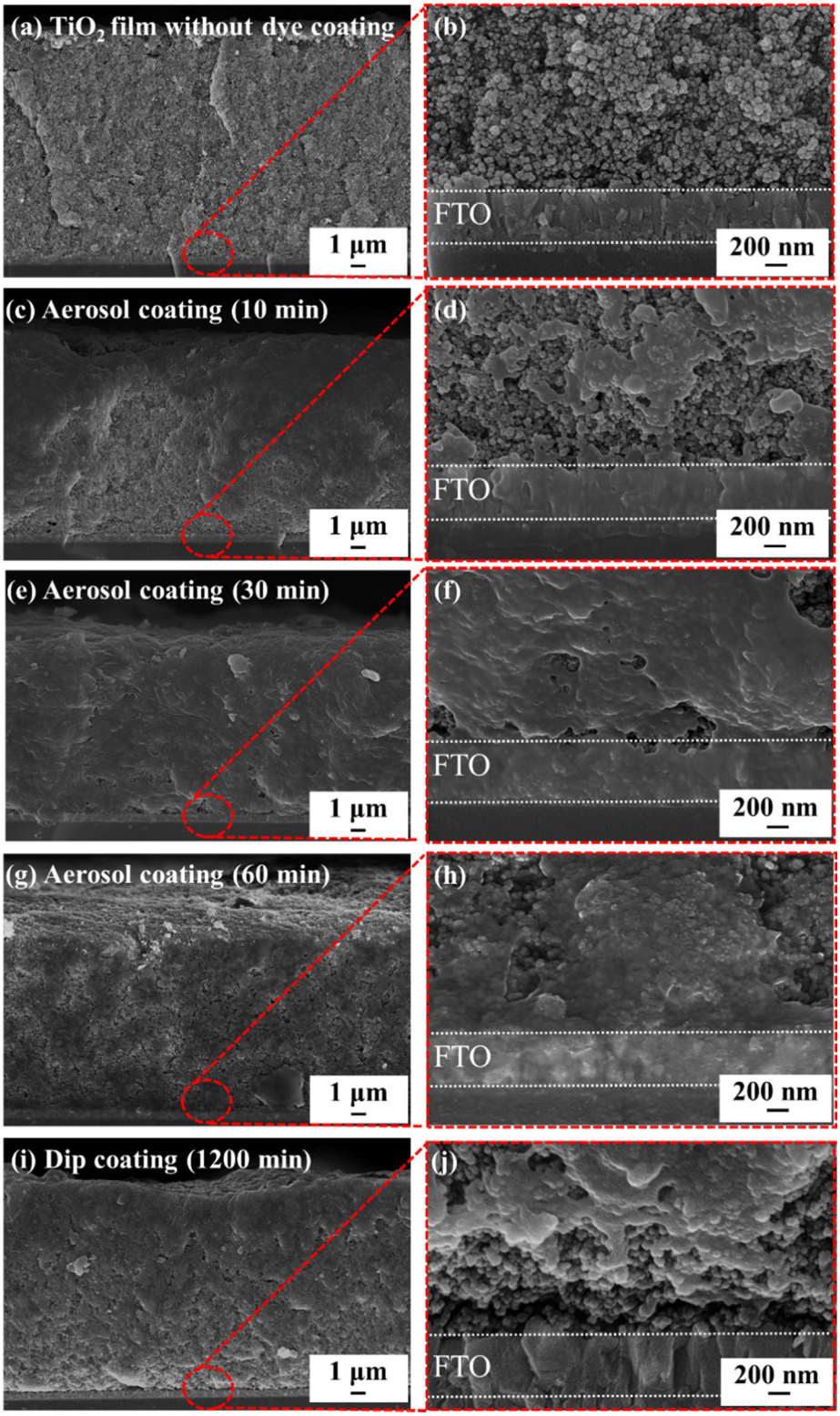

Fig. 4. Cross-sectional SEM images of (a, b) TiO_2 thin film without dye coating and TiO_2 thin films fabricated by aerosol coating for a duration of (c, d) 10 min, (e, f) 30 min, (g, h) 60 min, and (i, j) TiO_2 thin films fabricated by dip coating for a duration of 1200 min.

were sufficiently covered by the dye molecules. This suggests that the TiO_2 thin film in the photoelectrodes could be saturated by dye aerosol coating for $\geq \sim 30$ min. Fig. 4g and h illustrate the case of the TiO_2 thin film fabricated by aerosol coating for a duration of 60 min, and it can be clearly observed that the dye molecules were able to penetrate the TiO_2 thin film to reach the interface between the film and FTO glass. For comparison, SEM analysis of the TiO_2 thin film fabricated by dip coating process for 1200 min was also performed as shown in Fig. 4i and j. The top surface of the TiO_2 thin film seemingly adsorbed more dye molecules and the amount adsorbed in the depths was decreased to some extent. This suggests that the dye molecules were slowly diffused and adsorbed onto the TiO_2 NPs by a dye concentration gradient in the

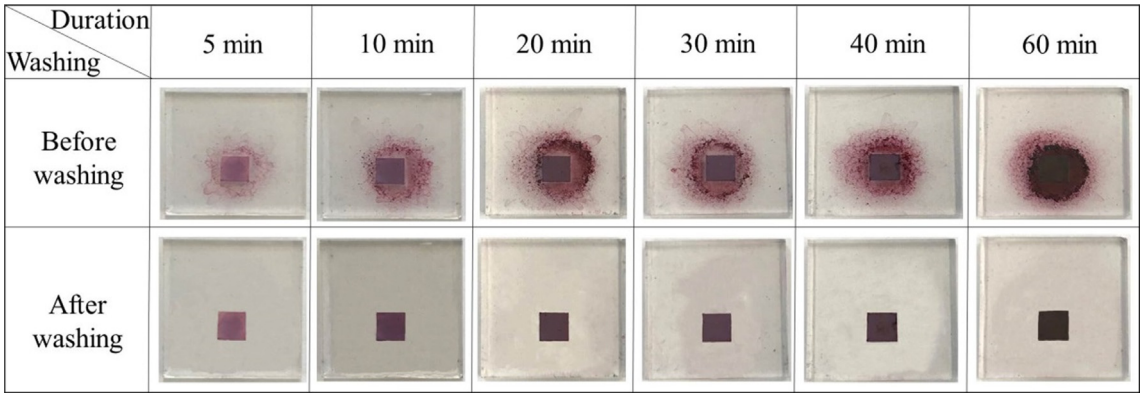

Fig. 5. Photographs of the TiO_2 thin film-based photoelectrodes fabricated by the dye aerosol coating method for durations of 5, 10, 20, 30, 40, and 60 min, respectively, before and after washing the redundant dye molecules deposited on the edges of the TiO_2 thin films. (The ratio between sheath and aerosol flow rates was fixed to 20:5.)

dip coating process. These results confirmed that the dye aerosol coating method developed in the present study is very effective and versatile for the rapid dye adsorption process in the manufacturing of DSSCs.

Fig. 5 shows the photographs of the surfaces of the TiO_2 thin films after the dye aerosol coating process performed for different durations. It was observed that the square-shaped photoactive areas made up with TiO_2 thin film were entirely covered by the impaction of the dye aerosols. As the dye aerosol coating duration was increased, the color of the TiO_2 thin film turned into dark purple, indicating that a larger amount of dye molecules were adsorbed. After 5 min of dye aerosol coating, the color of the TiO_2 thin film was pale pink, indicating that the majority of TiO_2 NPs could not sufficiently adsorb dye molecules owing to the relatively short coating duration. With the increase in the dye aerosol coating duration, the color of the TiO_2 thin film was gradually deepened. After the aerosol coating duration for 60 min, the excess dye molecules were accumulated on the surface edges of the TiO_2 NPs with a dark purple color. After each dye aerosol coating process, the TiO_2 thin film was washed with alcohol to remove the redundant dye molecules that were not attached to the surface of TiO_2 NPs. The photovoltaic performances of the DSSCs seemed to be almost saturated after dye aerosol coating duration for 30 min. The PCEs of DSSCs did not increase to any significant extent with the increasing duration of dye aerosol coating. Therefore, when the coating was prolonged, the excessive dye molecules became agglomerated at the surface of the TiO_2 thin films and deteriorated the photovoltaic performance of the DSSCs by hindering the electron transfer and simultaneously increasing the internal resistance.

The IPCE spectra were measured as a function of the incident light wavelength as shown in Fig. 6. The DSSCs fabricated by the dye aerosol coating method exhibited a better IPCE with the increasing duration of the dye aerosol coating process. The IPCE of DSSCs fabricated by dye aerosol coating for more than 20 min far exceeded that of DSSCs fabricated by dip coating for 1200 min. This result confirmed the effectiveness of the dye aerosol coating method, and its ability to rapidly adsorb dye molecules on thin films, while simultaneously improving the photovoltaic performances of the fabricated DSSCs.

Fig. 7a shows the comparison of the color and transparency of the DSSCs fabricated by both dip and aerosol coating methods for dye adsorption. It was clearly observed that the color of the DSSC fabricated via dye aerosol coating for 60 min was much darker in comparison with the DSSC fabricated via the dip coating process for 1200 min. This suggested that dye aerosol coating is an effective method to rapidly adsorb the dye molecules on TiO_2 thin films. Fig. 7b shows the comparison of the PCE values of DSSCs as a function of dip and aerosol coating duration. The highest PCE of the DSSC (7.28%) fabricated using the aerosol coating method was 23% higher than that of the DSSC

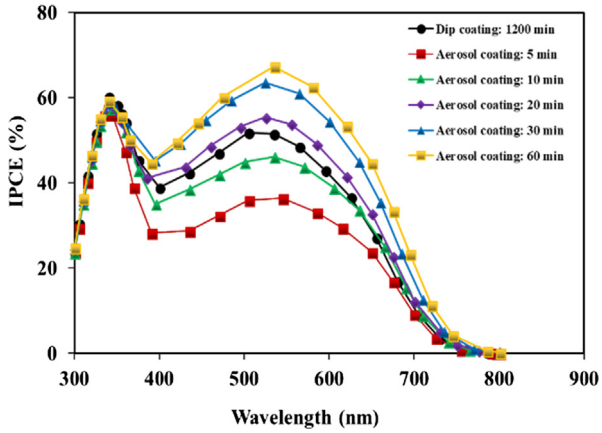

Fig. 6. Incident photon-electron conversion efficiency (IPCE) spectra of the DSSCs fabricated using (i) the dye aerosol coating method implemented for various coating durations (5–60 min) and (ii) the dip coating method applied for 1200 min for comparison.

fabricated using the conventional dip coating method (PCE = 5.92%). Moreover, the DSSCs fabricated using the single-stage dye aerosol impactor device designed in the present study were rapidly manufactured by significantly reducing the dye coating process with a production speed that was ~20 times as fast. Therefore, the single-stage dye aerosol impactor device could significantly accelerate the extent of dye adsorption and simultaneously increase the amount of dye so that it can inherently improve the photovoltaic performance of the DSSCs.

4. Conclusions

In this study, we have described an effective and versatile dye aerosol coating method, which can be compatible with any type of dye dispersed in solvent, using a single-stage aerosol impactor for rapid dye adsorption on the photoelectrodes of DSSCs. The results demonstrated that the amount and speed of dye adsorption on TiO_2 thin films in the photoelectrodes of DSSCs were increased considerably because of the inertial impaction of dye aerosol with strong momentum at a critical concentration. These attributes of the dye aerosol were precisely controlled by adjusting the mixing ratio of sheath gas and aerosol flow rates in the single-stage aerosol impactor. Using the specially designed accelerating nozzle and under optimized operating conditions of the single-stage aerosol impactor, the dye molecules were rapidly coated on the surface of the TiO_2 thin film and strongly bonded to the TiO_2 NPs. The photovoltaic performances of DSSCs fabricated by the dye aerosol coating method were found to be much better than those of the DSSCs

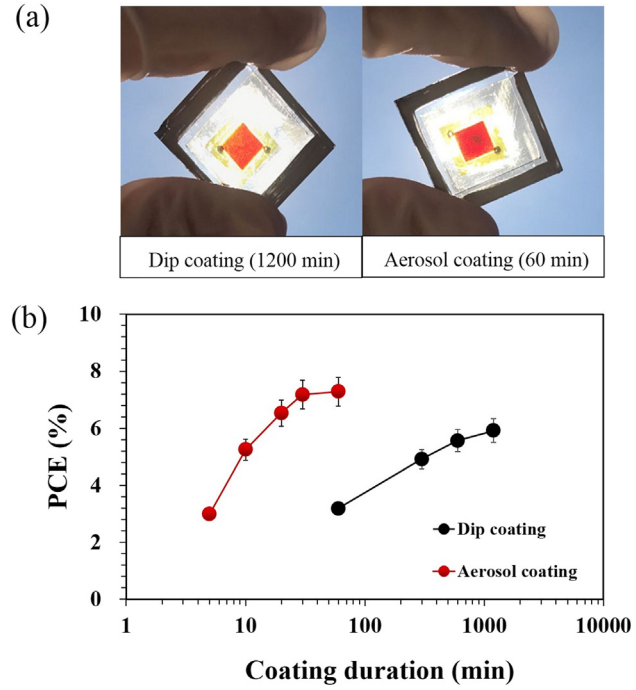

Fig. 7. (a) Photographs of DSSCs assembled using the dip coating process for 1200 min and dye aerosol coating process for 60 min. (b) Comparison of the PCEs of DSSCs fabricated following the dip- and aerosol-coating methods for different durations.

fabricated by the conventional dip coating method.

Acknowledgment

This research was supported by a grant from the National Research Foundation of Korea funded by the Ministry of Science and ICT (No. 2015R1A2A1A15054036).

References

O'Regan, B., Gratzel, M., 1991. A low-cost, high-efficiency solar cell based on dye sensitized colloidal TiO_2 films. Nature 353, 737–740.
Ahn, J.Y., Kim, J.H., Moon, K.J., Park, S.D., Kim, S.H., 2013. Synergistic effects of the aspect ratio of TiO_2 nanowires and multi-walled carbon nanotube embedment for enhancing photovoltaic performance of dye-sensitized solar cells. Nanoscale 5, 6842–6850.
Ahn, J.Y., Moon, K.J., Kim, J.H., Lee, S.H., Kang, J.W., Lee, H.W., Kim, S.H., 2014. Designed synthesis and stacking architecture of solid and mesoporous TiO_2 nanoparticles for enhancing the light-harvesting efficiency of dye-sensitized solar cells. ACS Appl. Mater. Interf. 6, 903–909.
Luo, X.T., Kim, J.H., Ahn, J.Y., Lee, D., Kim, J.M., Lee, D.G., Kim, S.H., 2016. Electrospraying-assisted rapid dye molecule uptake on the surfaces of TiO_2 nanoparticles for speeding up dye-sensitized solar cell fabrication. Sol. Energy Mater. Sol. Cells 144, 411–417.
Luo, X.T., Ahn, J.Y., Park, Y.S., Kim, J.M., Lee, H.W., Kim, S.H., 2017. Rapid fabrication and photovoltaic performance of Pt-free carbon nanotube counter electrodes of dye-sensitized solar cells. Sol. Energy 150, 13–19.
Latini, A., Cavallo, C., Aldibaja, F.K., Gozzi, D., 2013. Efficiency improvement of DSSC photoanode by scandium doping of mesoporous titania beads. J. Phys. Chem. C 117, 25276–25289.
Green, M.A., Emery, K., Hishikawa, Y., Warta, W., 2009. Solar cell efficiency tables (version 37). Prog. Photovolt:Res. Appl. 17, 85–92.
Liu, X.Z., Huang, Z., Li, K.X., Li, H., Li, D.M., Chen, L.Q., Meng, Q.B., 2006. Recombination reduction in dye-sensitized solar cells by screen-printed TiO_2 underlayers. Chin. Phys. Lett. 23 (9) 2606-2071.
Moon, K.J., Lee, S.W., Lee, Y.H., Kim, J.H., Ahn, J.Y., Lee, S.J., Lee, D.W., Kim, S.H., 2013. Effect of TiO_2 nanoparticle-accumulated bilayer photoelectrode and condenser lens-assisted solar concentrator on light harvesting in dye-sensitized solar cells. Nanoscale Res. Lett. 8, 283–290.
Lee, K.E., Gomez, M.A., Elouatik, S., Demopoulos, G.P., 2010. Further understanding of the adsorption mechanism of N719 sensitizer on anatase TiO_2 films for DSSC applications using vibrational spectroscopy and confocal Raman imaging. Langmuir 26 (16), 9575–9583.
Krkrek, A., Wang, D., Hou, Y., Zong, R., Thummel, R., 2006. Photosensitizers containing the 1,8-Naphthyridyl moiety and their use in dye-sensitized solar cells. Inorg. Chem. 45, 10131–10137.
Li, Q., Wu, J., Tang, Q.W., Lan, Z., Li, P.J., Lin, J.M., Fan, L.Q., 2008. Application of microporous polyaniline counter electrode for dye-sensitized solar cells. Electrochem. Commun. 10 (9), 1299–1302.
Ahn, J.Y., Kim, J.H., Kim, J.M., Lee, D., Kim, S.H., 2014. Multiwalled carbon nanotube thin films prepared by aerosol deposition process for use as highly efficient Pt-free counter electrodes of dye-sensitized solar cells. Sol. Energy 107, 660–667.
Wang, H., Hu, Y.H., 2012. Graphene as a counter electrode material for dye-sensitized solar cells. Energy Environ. Sci. 5 (8), 8182–8188.
Wu, J., Lan, Z., Hao, S., Li, P.J., Lin, J.M., Huang, M.L., Fang, L., Huang, Y., 2008. Progress on the electrolytes for dye-sensitized solar cells. Pure Appl. Chem. 80 (11), 2241–2258.
Ahn, J.Y., Cheon, H.K., Kim, W.D., Kang, Y.J., Kim, J.M., Lee, D.W., Cho, C.Y., Hwang, Y.H., Park, H.S., Kang, J.W., Kim, S.H., 2012. Aero-sol-gel synthesis and photovoltaic properties of mesoporous TiO_2 nanoparticles. Chem. Eng. J. 188, 216–221.
Yan, K., Qiu, Y., Chen, W., Zhang, M., Yang, S., 2011. A double layered photoanode made of highly crystalline TiO_2 nanooctahedra and agglutinated mesoporous TiO_2 microspheres for high efficiency dye sensitized solar cells. Energy Environ. Sci. 4 (6), 2168–2176.
Mohamed, I.M.A., Dao, V.-D., Yasin, A.S., Mousa, H.M., Mohamed, H.O., Choi, H.-S., Hassan, M.K., Barakat, N.A.M., 2016. Nitrogen-doped and SnO_2-incoporated TiO_2 nanofibers as novel and effective photoanode for enhanced efficiency dye-sensitized solar cells. Chem. Eng. J. 304, 48–60.
Yu, H., Zhang, S., Zhao, H., Xue, B., Liu, P., Will, G., 2009. High-performance TiO_2 photoanode with an efficient electron transport network for dye-sensitized solar cells. J. Phys. Chem. C 113 (36), 16277–16282.
Kim, B., Park, S.W., Kim, J.Y., Yoo, K., Lee, J.A., Lee, M.W., Lee, D.K., Kim, J.Y., Kim, B.S., Kim, H., Han, S., Son, H.J., Ko, M.J., 2013. Rapid dye adsorption via surface modification of TiO_2 photoanodes for dye-sensitized solar cells. ACS Appl. Mater. Interf. 5 (11), 5201–5207.
Hossain, M.A., Park, J., Ahn, J.Y., Park, C., Kim, Y., Kim, S.H., Lee, D., 2015. Investigation of TiO_2 nanotubes/nanoparticles stacking sequences to improve power conversion efficiency of dye-sensitized solar cells. Electrochimi. Acta 173, 665–671.
Wu, W.Q., Xu, Y.F., Su, C.Y., Kuang, D.B., 2014. Ultra-long anatase TiO_2 nanowire arrays with multi-layered configuration on FTO glass for high-efficiency dye-sensitized solar cells. Energy Environ. Sci. 7 (2), 644–649.
Wu, W.Q., Liao, J.Y., Chen, H.Y., Yu, X.Y., Su, C.Y., Kuang, D.B., 2012. Dye-sensitized solar cells based on a double layered TiO_2 photoanode consisting of hierarchical nanowire arrays and nanoparticles with greatly improved photovoltaic performance. J. Mater. Chem. 22 (34), 18057–18062.
Liao, J.Y., Lei, B.X., Kuang, D.B., Su, C.Y., 2011. Tri-functional hierarchical TiO_2 spheres consisting of anatase nanorods and nanoparticles for high efficiency dye-sensitized solar cells. Energy Environ. Sci. 4 (10), 4079–4085.
Su, T., Yang, Y., Shi, Y., Zhang, X., Jiang, Y., Fan, R., Cao, W., 2017. 40% enhanced photocurrent of dye sensitized solar cells using lotus-shaped H2-treated anatase TiO2 with 0 0 1 dominated facets. Chem. Eng. J. 316, 534–543.
Lee, J.H., Ahn, K., Kim, S.H., Jeong, S.Y., Bae, J.S., Hong, T.E., Cho, C.R., 2015. Efficiencies of dye-sensitized solar cells with hollow SnO_2 nanofiber/TiO_2 nanoparticle composite photoanodes. J. Nanosci. Nanotechnol. 15 (1), 244–247.
Jasim, K.E., 2011. Dye sensitized solar cells-working principles, challenges and opportunities. In: Solar Cells-Dye-Sensitized Devices. In Tech.
Tesfamichael, T., Will, G., Bell, J., Prince, K., Dytlewski, N., 2003. Characterization of a commercial dye-sensitized titania solar cell electrode. Sol. Energy Mater. Sol. Cells 76, 25–35.
Noda, S., Nagano, K., Inoue, E., Egi, T., Nakashima, T., Imawaka, N., Yoshino, K., 2009. Development of large size dye-sensitized solar cell modules with high temperature durability. Synthetic Met. 159 (21-22), 2355–2357.
Hinsch, A., Kroon, J.M., Kern, R., Uhlendorf, I., Holzbock, J., Meyer, A., Ferber, J., 2011. Long-term stability of dye-sensitized solar cells. Prog. Photovolt. Res. Appl. 9 (6), 425–438.
Marple, V.A., Klaus, W., 1976. Impactor design. Atmos. Environ. 10 (10), 891–896.
Mehdizadeh, E., Kumar, V., Pourkamali, S., Gonzales J., Abdolvand, R., A two stage agrosol impactor with embedded MEMS resonant mass balance for particulate size segregation and mass concentration monitoring. In: C. Sensors, IEEE. pp. 1–4.
Fuchs, N.A., 1989. The Mechanics of Aerosol. M. Dover Publications.
Rader, D.J., Marple, V.A., 1985. Effect of ultra-stokesian drag and particle interception in impaction characteristics. Aerosol. Sci. Technol. 4 (2), 141–156.
Hinds, W.C., 1999. Aerosol Technology: Properties, Behavior, and Measurement of Airborne Particles, second ed.
Slezakova, K., Morais S., do Carmo Pereira, M., 2012. Indoor Air Pollutants: Relevant Aspects and Health Impacts, Environmental Health-Emerging Issues and Practice.
Newton, G.J., Raabe, O.G., Mokler, B.V., 1997. Cascade impactor design and performance. J. Aerosol. Sci. 8, 339–347.
Kuo, H.P., Wu, C.T., 2014. Speed up dye-sensitized solar cell fabrication by rapid dye solution droplets bombardment. Sol. Energy Mater. Sol. Cells 120, 81–86.
Angelis, F.D., Fantacci, S., Selloni, A., Nazeeruddin, M.K., Grätzel, M., 2010. First-principles modeling of the adsorption geometry and electronic structure of Ru (II) dyes on extended TiO_2 substrates for dye-sensitized solar cell application. J. Phys. Chem. C 114 (3), 6054–6061.
Yu, H., Zhang, S.Q., Zhao, H., Zhang, H., 2010. Photoelectrochemical quantification of electron transport resistance of TiO_2 photoanodes for dye-sensitized solar cells. Phys. Chem. Chem. Phys. 12, 6625–6631.
Bisquert, J., Santiago, F.F., Seró, I.M., Belmonte, G.G., Gime´nez, S., 2009. Electron lifetime in dye-sensitized solar cells: theory and interpretation of measurements. J. Phys. Chem. C 113, 17278–17290.
Ha, S.H., Yu, H.W., Jang, N.S., Kim, J.H., Kim, S.H., Kim, J.M., 2016. Compact and high-power dye-sensitized solar system integrated with low-cost solar-concentrating polymer lens. Sol. Energy Mater. Sol. Cells 155, 362–367.